On Srinivasan's Criterion for the Vapor Pressure Curve†

Santiago Velasco,*,‡ Francisco L. Román,§ and Juan A. White‡

Departamento de Física Aplicada, Universidad de Salamanca, 37008 Salamanca, Spain, and Departamento de Física Aplicada, Escuela Politécnica Superior de Zamora, Universidad de Salamanca, 49022 Zamora, Spain

Srinivasan's criterion states that, for all pure fluids, the saturation functions $\phi_1 = (1 - T_r)P_r$ and $\phi_1^* = (1 - P_r)T_r$ (with $T_r = T/T_c$ and $P_r = P/P_c$, T_c and P_c being the temperature and pressure at the critical point) in the vapor−liquid coexistence region present maxima at two different temperatures T_{r1} and T_{r1}^* within a small spread of values: $T_{r1} \approx 0.85$ to 0.9 and $T_{r1}^* \approx 0.71$ to 0.76. In this paper, we study this criterion for 51 fluids, including quantum fluids (^{3}He, ^{4}He, and H_2) and normal alkanes C_nH_{2n+2} with $n \leq 40$. We find that $T_{r1} \approx 0.77$ to 0.93 and $T_{r1}^* \approx 0.64$ to 0.82. Correlations between the values of these maxima, (T_{r1}, $\phi_{1,\max}$) and (T_{r1}^*, $\phi_{1,\max}^*$), are derived depicting their mutual dependence. We also find that the values of the maxima can be accurately predicted in terms of the Pitzer acentric factor ω. These predictions are checked against additional data for 1214 fluids.

Introduction

The vapor pressure curve provides the relation between temperature and pressure of a fluid in the liquid−vapor coexistence region. This curve extends from the triple point to the critical point, and its shape has been the object of thermodynamics research for about 175 years since Clapeyron proposed his famous equation. A plethora of equations have been reported in the literature to correlate or to predict vapor pressure experimental data. In this long way, several criteria/conditions have been proposed to check thermodynamic consistency of the used equations. Perhaps, the more known and used criteria are Waring's criterion and the two Riedel conditions. Waring's criterion[1] states that $-d(\ln P_r)/d(1/T_r)$ (with $T_r = T/T_c$ and $P_r = P/P_c$, T_c and P_c being the temperature and pressure at the critical point) presents a minimum at a reduced temperature around $T_r \approx 0.80$ to 0.85. The first Riedel condition[2] states that the quantity $\alpha_c = (dP_r/dT_r)_{T_r=1}$ is a characteristic constant for each fluid (Riedel's factor), typically in the range 5 to 8. The second Riedel condition, also known as the Plank−Riedel condition,[3] states that $(d\alpha/dT_r)_{T_r=1} = 0$ with $\alpha = d(\ln P_r)/d(\ln T_r)$. Strictly, this condition is at odds with renormalization-group theory which predicts that d^2P_r/dT_r^2 should diverge at the critical point, and therefore, it must be substituted by the condition that the Riedel function $\alpha(T_r)$ presents a minimum at a reduced temperature close to the critical value $T_r = 1$.

Some years ago, analyzing the vapor pressure curve for methane and refrigerants R123 and R134a, Khan and Srinivasan[4–6] found that the functions $\phi_1 = (1 - T_r)P_r$ and $\phi_1^* = (1 - P_r)T_r$ exhibit maxima at two different reduced temperatures, T_{r1} and T_{r1}^*, with $T_{r1}^* < T_{r1}$. More recently, this fact was analyzed more systematically by Srinivasan[7] for 55 fluids ranging from monatomic liquids to polar high boiling point liquids. Three main conclusions can be derived from Srinivasan's study: (1) the values of T_{r1} and T_{r1}^* occur in a narrow band: $T_{r1} \approx 0.85$ to 0.9 and $T_{r1}^* \approx 0.71$ to 0.76; (2) the values of T_{r1} and T_{r1}^* seem to increase with the molecular complexity of the fluid; and (3) there exists a linear relation between the maximum values of these functions, $\phi_{1,\max} = \phi_1(T_{r1})$ and $\phi_{1,\max}^* = \phi_1^*(T_{r1}^*)$. Very recently, Tian et al.[8] have used a hard-sphere equation of state with a Redlich−Kwong attractive term to analyze T_{r1} and $\phi_{1,\max}$.

The aim of this work is to extend Srinivasan's study in two directions. The first is to include in the analysis some quantum fluids (^{3}He, ^{4}He, and H_2) and normal alkanes C_nH_{2n+2} with a high carbon number ($n \leq 40$), to check or to amplify Srinivasan's conclusions. The second is to analyze more quantitatively the dependence of the different maxima with the molecular complexity by choosing the Pitzer acentric factor ω as an indicator of such complexity[9]

$$\omega = -1.0 - \log_{10} P_r \quad \text{at } T_r = 0.7 \tag{1}$$

Besides its intrinsic interest as a guide to check the precision of experimental vapor data, Srinivasan's points present the peculiarity that one can obtain the slope of the vapor pressure curve, $P_r' = dP_r/dT_r$, at such points in terms of the temperature and pressure of the points. This property makes Srinivasan's points very useful as reference points. For example, Velasco et al.[10,11] have recently proposed a method to estimate the two first critical amplitudes for the simplest scaling vapor pressure equation in terms of the reduced temperature T_{r1} and pressure P_{r1} of the maximum of the function $\phi_1 = (1 - T_r)P_r$. Furthermore, we remark that the experimental determination of Srinivasan's points is rather accessible because they are far enough from the critical point to avoid the usual difficulties (thermal stability, gravity effects, and impurity effects) associated to experimental measurements in the critical region.

Srinivasan's Criterion

Figure 1(a) and Figure 1(b) show a typical variation of $\phi_1 = (1 - T_r)P_r$ and $\phi_1^* = (1 - P_r)T_r$, respectively, with T_r for three common fluids (argon, water, and methanol) from the vapor pressure data reported in the NIST Webbook.[12] These plots show that $\phi_1(T_r)$ and $\phi_1^*(T_r)$ present maxima at different, fluid-dependent reduced temperatures T_{r1} and T_{r1}^*, respectively, with $T_{r1}^* < T_{r1}$.

† Part of the "Sir John S. Rowlinson Festschrift".

* To whom correspondence should be addressed. E-mail: santi@usal.es.
‡ Salamanca.
§ EPS Zamora.

10.1021/je100392h
Published on Web 06/16/2010

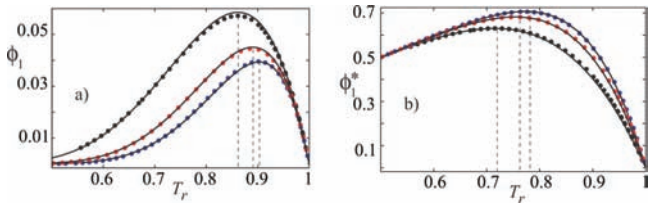

Figure 1. Variation of the saturation functions $\phi_1(T_r) = (1 - T_r)P_r$ (a) and $\phi_1^*(T_r) = (1 - P_r)T_r$ (b) with T_r for Ar (black), H_2O (red), and methanol (blue). Vapor pressure data were obtained from the NIST Webbook.[12] Solid lines correspond to functions $\phi_1(T_r)$ and $\phi_1^*(T_r)$ with vapor pressure obtained from the Clausius−Clapeyron equation [eq 2 of the Supporting Information].

The fact that $\phi_1(T_r)$ goes through a maximum at T_{r1} is mathematically expressed by the relation

$$\left[\frac{d\phi_1(T_r)}{dT_r}\right]_{T=T_{r1}} = -P_{r1} + (1 - T_{r1})\left(\frac{dP_r}{dT_r}\right)_{T=T_{r1}} = 0 \tag{2}$$

where $P_{r1} = P_r(T_{r1})$. From eq 2, one obtains

$$P'_{r1} \equiv \left(\frac{dP_r}{dT_r}\right)_{T=T_{r1}} = \frac{P_{r1}}{1 - T_{r1}} = \frac{\phi_{1,max}}{(1 - T_{r1})^2} \tag{3}$$

with $\phi_{1,max} \equiv \phi_1(T_{r1}) = (1 - T_{r1})P_{r1}$.

On the other hand, the fact that $\phi_1^*(T)$ goes through a maximum at T_{r1}^* implies that

$$\left[\frac{d\phi_1^*(T_r)}{dT_r}\right]_{T=T_{r1}^*} = -T_{r1}^*\left(\frac{dP_r}{dT_r}\right)_{T=T_{r1}^*} + (1 - P_{r1}^*) = 0 \tag{4}$$

where $P_{r1}^* = P_r(T_{r1}^*)$. From eq 4, one obtains

$$P_{r1}^{*\prime} \equiv \left(\frac{dP_r}{dT_r}\right)_{T=T_{r1}^*} = \frac{1 - P_{r1}^*}{T_{r1}^*} = \frac{\phi_{1,max}^*}{T_{r1}^{*2}} \tag{5}$$

with $\phi_{1,max}^* \equiv \phi_1^*(T_{r1}^*) = (1 - P_{r1}^*)T_{r1}^*$.

Equations 3 and 5 show that the slopes of the vapor pressure curve at Srinivasan's points can be obtained in terms of the reduced temperature and pressure of such points.

All Srinivasan's parameters can be derived from a suitable vapor pressure equation. In the Supporting Information, a direct estimation of these parameters is made from the Clausius−Clapeyron (CC) equation.

Results and Discussion

We have analyzed the $\phi_1(T_r)$ and $\phi_1^*(T_r)$ functions for the 51 substances listed in Table 1 of the Supporting Information (SI). For ^{3}He and ^{4}He, vapor pressure data were obtained from the corresponding ITS-90 vapor pressure equation.[13−15] For normal alkanes C_nH_{2n+2} with $n = 20$, 30, and 40, vapor pressure data were obtained from the Lemmon−Goodwin vapor pressure equation.[16] For the remaining fluids, vapor pressure data were recorded from the NIST Webbook.[12] The choice of these fluids is based in the same criterium as that of Srinivasan[7] so that a representative sampling of monatomic liquids, hydrocarbons, refrigerants, and cryogenic liquids is considered. The obtained values for T_{r1}, $\phi_{1,max}$, T_{r1}^*, and $\phi_{1,max}^*$ are also given in Table 1 of the SI. The fluids are ordered with increasing values of the Pitzer acentric factor ω, which is usually considered as an indicator of the molecular complexity of a fluid. The values of T_{r1} vary between $T_{r1} = 0.7743$ for ^{3}He and $T_{r1} = 0.9314$ for tetracontane ($C_{40}H_{82}$). The values of T_{r1}^* vary between $T_{r1}^* = 0.6420$ for ^{3}He and $T_{r1}^* = 0.8147$ for tetracontane. These values enlarge the ranges reported by Srinivasan for T_{r1} and T_{r1}^* and suggest that both T_{r1} and T_{r1}^* tend to 1 when ω increases, in agreement with the results obtained with the CC equation [eq 2 of the SI].

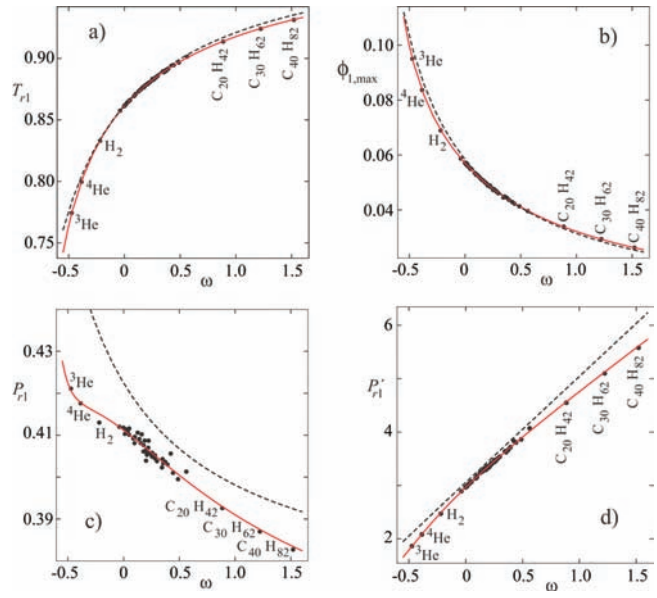

Figure 2. (a) Plot of T_{r1} vs ω for fluids given in Table 1 of the SI. The dashed line corresponds to the Clausius−Clapeyron result [eq 6 of the SI]. The solid line is a fit to the data [eq 6]. (b) Plot of $\phi_{1,max}$ vs ω for fluids given in Table 1 of the SI. The dashed line corresponds to the Clausius−Clapeyron result [eq 8 of the SI]. The solid line is a fit to the data [eq 7]. (c) Plot of $P_{r1} = \phi_{1,max}/(1 - T_{r1})$ vs ω for fluids given in Table 1 of the SI. The dashed line corresponds to the Clausius−Clapeyron result [eq 7 of the SI]. The solid line corresponds to P_{r1} using eqs 6 and 7. (d) Plot of $P'_{r1} = \phi_{1,max}/(1 - T_{r1})^2$ vs ω for fluids given in Table 1 of the SI. The dashed line corresponds to the Clausius−Clapeyron result [eq 9 of the SI]. The solid line corresponds to P'_{r1} using eqs 6 and 7.

Figure 2 shows plots of T_{r1}, $\phi_{1,max}$, $P_{r1} = \phi_{1,max}/(1 - T_{r1})$, and $P'_{r1} = \phi_{1,max}/(1 - T_{r1})^2$ vs ω. Symbols correspond to NIST data using the values reported in the forth and fifth columns of Table 1 of the SI. Dashed lines correspond to theoretical results obtained from the CC equation [eqs 6 to 9 of the SI]. Equation 6 of the SI predicts T_{r1} values with an average relative deviation (ARD) of 0.17 % with respect to those reported in Table 1 of the SI, while eq 8 of the SI predicts $\phi_{1,max}$ values with an ARD of 1.46 % with respect to those reported in Table 1 of the SI. On the other hand, eq 7 of the SI predicts the NIST P_{r1} values with an ARD of 2.31 %, while eq 9 of the SI predicts the NIST P'_{r1} values with an ARD of 3.60 %. The main discrepancies between experimental and theoretical CC results appear for negative ω values (quantum fluids) and large positive ω values (alkanes with a high carbon number).

To obtain accurate empirical correlations between the acentric factor ω and the values of T_{r1} and $\phi_{1,max}$ characterizing the maximum of the function $\phi_1(T_r)$, we have performed a regression analysis of the data reported in Table 1 of the SI. We have found the following relations

$$T_{r1} = 1 - \frac{0.13864}{1 + \omega} - \frac{0.07911\omega}{(1.47977 + \omega)^2} \tag{6}$$

and

$$\phi_{1,\max} = \frac{0.07398}{1+\omega} - \frac{0.02188}{(1+\omega)^2} + \frac{0.00491}{(1+\omega)^3} \qquad (7)$$

Equations 6 and 7 are plotted by solid red lines in Figure 2(a) and Figure 2(b), respectively. Equation 6 fits the T_{r1} values of Table 1 of the SI with an ARD of 0.028 %, while eq 7 fits the $\phi_{1,\max}$ values of Table 1 of the SI with an ARD of 0.22 %. For $\omega = 0$, eq 7 gives $T_{r1}^{(0)} = 0.86136$, while eq 7 gives $\phi_{1,\max}^{(0)} = 0.05701$, very close to the values obtained with the CC equation. Furthermore, when $\omega \rightarrow \infty$, eq 6 gives $T_{r1}^{(\infty)} = 1$ and eq 7 gives $\phi_{1,\max}^{(\infty)} = 0$, in agreement with the same limit values obtained with the CC equation.

From eqs 6 and 7, one can obtain the ω-dependence of $P_{r1} = \phi_{1,\max}/(1 - T_{r1})$ and, using eq 3, of P'_{r1}. These dependences are plotted in Figure 2(c) and Figure 2(d), respectively, by solid red lines. The empirical correlations fit the NIST P_{r1} values with an ARD of 0.21 % and the NIST P'_{r1} values with an ARD of 0.37 %. We note that the maximum positive deviations in Figure 2(c) correspond to R41 (0.75 %) and to H_2 (0.51 %), while the maximum negative deviations correspond to 12-fluoropentane (−0.99 %), N_2O (−0.59 %), CO_2 (−0.57 %), and methanol (−0.55 %).

Figure 3 shows plots of T_{r1}^*, $\phi_{1,\max}^*$, $P_{r1}^* = 1 - (\phi_{1,\max}^*/T_{r1}^*)$, and $P_{r1}^{*'} = \phi_{1,\max}^*/T_{r1}^{*2}$ vs ω. Symbols correspond to NIST data using the values reported in the sixth and seventh columns of Table 1 of the SI. Dashed lines correspond to theoretical results obtained from the CC equation [eqs 10 to 13 of the SI]. Equation 11 of the SI predicts T_{r1}^* values with an average relative deviation (ARD) of 0.31 % with respect to those reported in Table 1 of the SI, while eq 12 of the SI predicts $\phi_{1,\max}^*$ values with an ARD of 0.16 % with respect to those reported in Table 1 of the SI. On the other hand, eq 10 of the SI predicts the NIST P_{r1}^* values with an ARD of 1.58 %, while eq 13 of the SI predicts the NIST $P_{r1}^{*'}$ values with an ARD of 0.60 %. Again, the main discrepancies between experimental and theoretical CC results arise for negative ω values (quantum fluids) and large positive ω values (alkanes with a high carbon number).

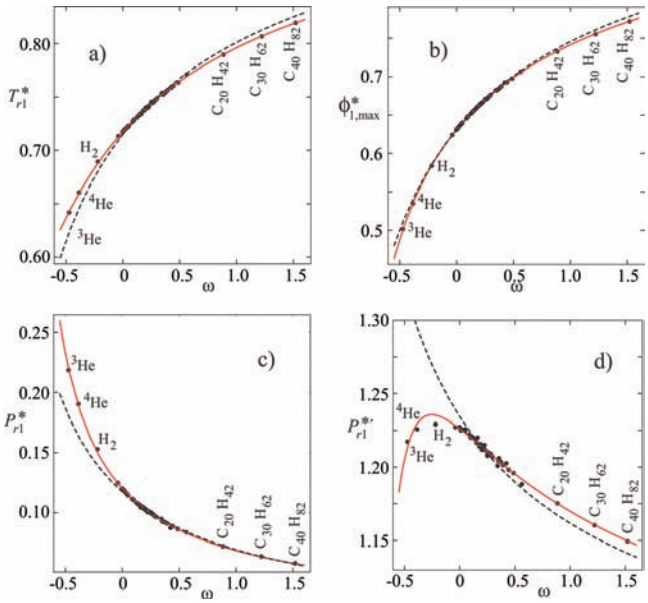

Figure 3. (a) Plot of T_{r1}^* vs ω for fluids given in Table 1 of the SI. The dashed line corresponds to the Clausius−Clapeyron result [eq 11 of the SI]. The solid line is a fit to the data [eq 8]. (b) Plot of $\phi_{1,\max}^*$ vs ω for fluids given in Table 1 of the SI. The dashed line corresponds to the Clausius−Clapeyron result [eq 12 of the SI]. The solid line is a fit to the data [eq 9]. (c) Plot of $P_{r1}^* = 1 - (\phi_{1,\max}^*/T_{r1}^*)$ vs ω for fluids given in Table 1 of the SI. The dashed line corresponds to the Clausius−Clapeyron result [eq 10 of the SI]. The solid line corresponds to P_{r1}^* using eqs 8 and 9. (d) Plot of $P_{r1}^{*'} = \phi_{1,\max}^*/T_{r1}^{*2}$ vs ω for fluids given in Table 1 of the SI. The dashed line corresponds to the Clausius−Clapeyron result [eq 13 of the SI]. The solid line corresponds to $P_{r1}^{*'}$ using eqs 8 and 9.

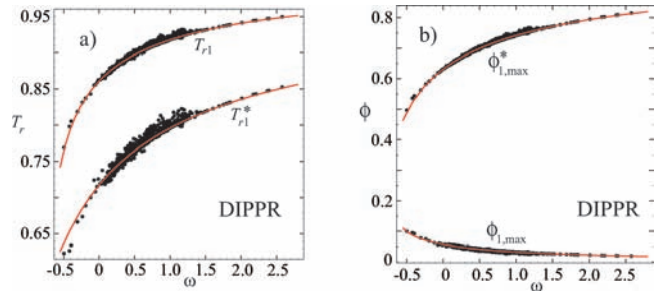

Figure 4. (a) Reduced temperatures T_{r1} and T_{r1}^* vs the acentric factor ω. Lines correspond to the proposed empirical correlations [eqs 6 and 8]. (b) A plot of $\phi_{1,\max}$ and $\phi_{1,\max}^*$ vs the acentric factor ω. Lines correspond to the proposed empirical correlations [eqs 7 and 9]. The symbols correspond to 1214 DIPPR fluids with accepted data for T_c and P_c.

To obtain accurate empirical correlations between the acentric factor ω and the values of T_{r1}^* and $\phi_{1,\max}^*$ characterizing the maximum of the function $\phi_1^*(T_r)$, we have performed a regression analysis of the data reported in Table 1 of the SI. We have found the following relations

$$T_{r1}^* = 1 - \frac{0.28246 + 0.16318\ln(1+\omega) + 0.02546[\ln(1+\omega)]^2}{1+\omega} \qquad (8)$$

and

$$\phi_{1,\max}^* = 1 - \frac{0.36873 + 0.18868\ln(1+\omega) + 0.03674[\ln(1+\omega)]^2}{1+\omega} \qquad (9)$$

Equations 8 and 9 are plotted by solid red lines in Figure 3(a) and Figure 3(b), respectively. Equation 8 fits the T_{r1}^* values of Table 1 of the SI with an ARD of 0.056 %, while eq 9 fits the $\phi_{1,\max}^*$ values of Table 1 of the SI with an ARD of 0.040 %. For $\omega = 0$, eq 8 gives $T_{r1}^{*(0)} = 0.71754$, while eq 9 gives $\phi_{1,\max}^{*(0)} = 0.63127$, also very close to the values obtained with the CC equation. Furthermore, when $\omega \rightarrow \infty$, eq 8 gives $T_{r1}^{*(\infty)} = 1$ and eq 9 gives $\phi_{1,\max}^{*(\infty)} = 1$, in agreement with the same limit values obtained with the CC equation.

From eqs 8 and 9, one can obtain the ω-dependence of $P_{r1}^* = 1 - (\phi_{1,\max}^*/T_{r1}^*)$ and, using eq 5, of $P_{r1}^{*'}$. These dependences are plotted in Figure 3(c) and Figure 3(d), respectively, by solid red lines. The empirical correlations fit the NIST P_{r1}^* values with an ARD of 0.44 % and the NIST $P_{r1}^{*'}$ values with an ARD of 0.10 %.

To check eqs 6 to 9, we have considered 1214 substances with data reported by DIPPR.[17] These substances were chosen among those for which DIPPR provides accepted data for T_c and P_c. The corresponding values of T_{r1}, $\phi_{1,\max}$, T_{r1}^*, and $\phi_{1,\max}^*$ were obtained by calculating the maxima of $\phi_1(T_r)$ and $\phi_1^*(T_r)$, with P_r given by a generalized Riedel equation.[2,18] The values for the acentric factor ω were also obtained from the Riedel equation using eq 8. The values of T_{r1} and T_{r1}^* against ω are plotted in Figure 4(a) together with eqs 6 and 8. Equation 6 predicts T_{r1} with an overall ARD of 0.13 %, while eq 8 predicts T_{r1}^* with an overall ARD of 0.36 %. The values of $\phi_{1,\max}$ and $\phi_{1,\max}^*$ against ω are plotted in Figure 4(b) together with eqs 7 and 9. Equation 7 predicts $\phi_{1,\max}$ with an overall ARD of 2.57

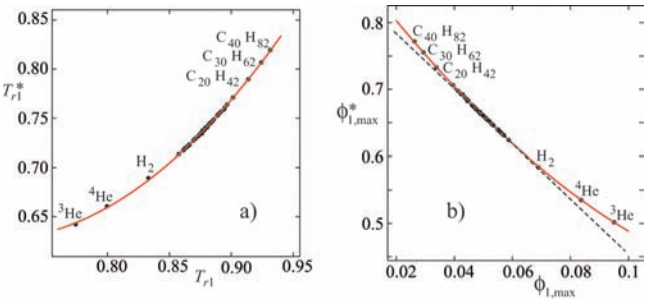

Figure 5. (a) Plot of T^*_{r1} vs T_{r1} for fluids given in Table 1 of the SI. The red line corresponds to a fit to the data [eq 10]. (b) Plot of $\phi^*_{1,max} = (1 - P^*_{r1})T^*_{r1}$ vs $\phi_{1,max} = (1 - T_{r1})P_{r1}$ for fluids given in Table 1 of the SI. The solid red line corresponds to a fit to the data [eq 12]. The dashed line corresponds to Srinivasan's linear correlation[7] [eq 11].

%, while eq 9 predicts $\phi^*_{1,max}$ with an overall ARD of 0.20 %. It should be remarked that the DIPPR values for T_c and P_c are given for many substances with errors up to 25 %.

Figure 5(a) and Figure 5(b) show a plot of T^*_{r1} vs T_{r1} and $\phi^*_{1,max}$ vs $\phi_{1,max}$, respectively, for the fluids of Table 1 of the SI. These figures indicate that there exists a clear correlation between them. We have found that, for the fluids considered in Table 1 of the SI, a simple and accurate empirical relation between T_{r1} and T^*_{r1} is given by

$$T^*_{r1} = 2.5295 - 5.3869T_{r1} + 3.8115T^2_{r1} \qquad (10)$$

with an ARD of 0.056 %, a maximum positive deviation (0.24 %) for ^{3}He, and a maximum negative deviation (−0.33 %) for H_2. Equation 10 is plotted in Figure 5(a) by a solid red line.

On the other hand, by excluding quantum fluids (^{3}He, ^{4}He, and H_2) and alkanes C_nH_{2n+2} with $n > 8$, Srinivasan[7] found a linear relation between the two maxima

$$\phi^*_{1,max} = \frac{0.2095 - \phi_{1,max}}{0.2415} = 0.8675 - 4.1408\phi_{1,max} \qquad (11)$$

which is plotted in Figure 5(b) by a dashed line. If the quantum fluids and alkanes C_nH_{2n+2} with $n > 8$ are included in the correlation, eq 11 gives an ARD of 0.31 %, with the maximum positive deviation (0.21 %) for R41 and the maximum negative deviation (−5.5 %) for ^{3}He. We have found that for the fluids considered in Table 1 of the SI a more accurate empirical relation between $\phi_{1,max}$ and $\phi^*_{1,max}$ is given by

$$\phi^*_{1,max} = 0.9148 - 5.9235\phi_{1,max} + 16.5904\phi^2_{1,max} \qquad (12)$$

with an ARD of 0.07 %, maximum positive deviation (0.25 %) for water, and maximum negative deviation (−0.18 %) for 12-fluoropentane. Equation 12 is plotted in Figure 5(b) by a solid red line.

Conclusions

Srinivasan's criterion states that there exists a maximum in the functions $\phi^*_1 = (1 - P_r)T_r$ and $\phi_1 = (1 - T_r)P_r$ along the vapor pressure curve $P_r = P_r(T_r)$ for all pure fluids. We have extended Srinivasan's study by including quantum fluids (^{3}He, ^{4}He, and H_2) and alkanes C_nH_{2n+2} with a high carbon number ($n = 20$, 30, and 40). This extension allows one to obtain new equations for the correlations between two maxima. In particular, we propose a set of equations for obtaining Srinivasan's maxima in terms of the acentric factor ω. These equations provide very nice examples of the Pitzer three-parameter corresponding state theory, and they can then be used either for predicting purposes or for testing experimental vapor pressure data.

Supporting Information Available:

Derivation of Srinivasan's parameters from the Clausius−Clapeyron equation. Table of the critical parameters, Srinivasan's values, and acentric factor for the substances considered in this work. This material is available free of charge via the Internet at http://pubs.acs.org.

Literature Cited

(1) Waring, W. Form of a Wide-Range Vapor Pressure Equation. *Ind. Eng. Chem.* **1954**, *46*, 762–763.
(2) Riedel, L. A new universal vapor pressure formula. *Chem. Eng. Technol.* **1954**, *26*, 83–89.
(3) Plank, R.; Riedel, L. A New Criterion for the Curves of the Vapor Pressure at the Critical Point. *Ing. Arch.* **1948**, *16*, 255–266.
(4) Khan, S.; Srinivasan, K. A correlation method for data on saturation thermodynamic properties and its application to methane. *High Temp.-High Pressures* **1994**, *26*, 427–438.
(5) Khan, S.; Srinivasan, K. Saturation equilibrium and slope properties of R-123. *High Temp.-High Pressures* **1994**, *26*, 519–530.
(6) Khan, S.; Srinivasan, K. Inter-related p - T and ρ - T equations for saturated fluid phases: application to R-134a. *J. Phys. D: Appl. Phys.* **1996**, *29*, 3079–3088.
(7) Srinivasan, K. An Interesting Feature of the Vapor Pressure Curve. *Z. Phys. Chem.* **2002**, *216*, 1379–1387.
(8) Tian, J.; Jiang, H.; Xu, Y. A property of the saturated vapor pressure: Results from equations of state. *Mod. Phys. Lett. B* **2009**, *23*, 3091–3096.
(9) Pitzer, K. S.; Lippmann, D. Z.; Curl, R. F.; Huggins, C. M.; Petersen, D. E. The Volumetric and Thermodynamic Properties of Fluids. II. Compressibility Factor, Vapor Pressure and Entropy of Vaporization. *J. Am. Chem. Soc.* **1955**, *77*, 3433–3440.
(10) Velasco, S.; Roman, F. L.; White, J. A.; Mulero, A. Vapor pressure critical amplitudes from the normal boiling point. *Appl. Phys. Lett.* **2007**, *90*, 141905-1-3.
(11) Velasco, S.; Roman, F. L.; White, J. A. ^{3} He Vapor Pressure near Its Critical Point. *J. Low Temp. Phys.* **2008**, *152*, 177–185.
(12) *NIST Chemistry WebBook*; Linstrom, P. J., Mallard, W. G., Eds.; NIST Standar Reference Database Number 69, July 2002 (http://webbook.nist.gov).
(13) Preston-Thomas, H. The International Temperature Scale of 1990 (ITS-90). *Metrologia* **1990**, *27*, 3–10.
(14) Preston-Thomas, H. The International Temperature Scale of 1990 (ITS-90) (erratum). *Metrologia* **1990**, *27*, 107.
(15) McGlashan, M. L. The International Temperature Scale of 1990 (ITS-90). *J. Chem. Thermodyn.* **1990**, *22*, 653–663.
(16) Lemmon, E. W.; Goodwin, A. R. H. Critical Properties and Vapor Pressure Equation for Alkanes C_nH_{2n+2}: Normal Alkanes With $n \leq 36$ and Isomers for $n = 4$ Through $n = 9$. *J. Phys. Chem. Ref. Data* **2000**, *29*, 1–39.
(17) American Institute of Chemical Engineers. *Design Institute for Physical Property Data (DIPPR) files*, Version 17.0; Technical Database Services, Inc. (www.tds.cc).
(18) Vetere, A. Again the Riedel equation. *Fluid Phase Equilib.* **2006**, *240*, 155–160.

Received for review April 21, 2010. Accepted June 4, 2010. We thank financial support by Ministerio de Educación y Ciencia of Spain under Grant FIS2009-07557.

JE100392H